

Advancing Peptide-Based Biorecognition Elements for Biosensors Using *in-Silico* Evolution

Xingqing Xiao,[†] Zhifeng Kuang,[‡] Joseph M. Slocik,[‡] Sirimuvva Tadepalli,^{||} Michael Brothers,[§] Steve Kim,[§][¶] Peter A. Mirau,[‡][¶] Claire Butkus,[‡] Barry L. Farmer,[‡] Srikanth Singamaneni,^{||} Carol K. Hall,^{*,†}[¶] and Rajesh R. Naik^{*,§}[¶]

[†]Department of Chemical and Biomolecular Engineering, North Carolina State University, Raleigh, North Carolina 27695, United States

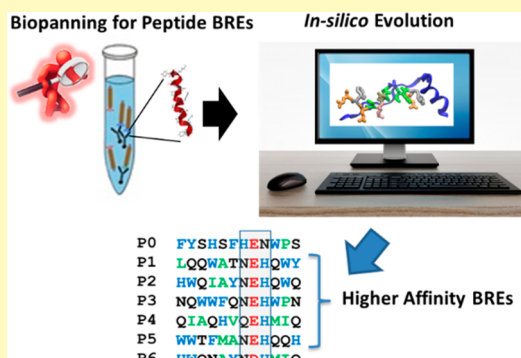
[‡]Materials and Manufacturing Directorate and [§]711th Human Performance Wing, Air Force Research Laboratory, Wright-Patterson Air Force Base, Dayton, Ohio 45433, United States

^{||}Department of Mechanical Engineering and Materials Science, Institute of Materials Science and Engineering, Washington University in St. Louis, St. Louis, Missouri 63130, United States

S Supporting Information

ABSTRACT: Sensors for human health and performance monitoring require biological recognition elements (BREs) at device interfaces for the detection of key molecular biomarkers that are measurable biological state indicators. BREs, including peptides, antibodies, and nucleic acids, bind to biomarkers in the vicinity of the sensor surface to create a signal proportional to the biomarker concentration. The discovery of BREs with the required sensitivity and selectivity to bind biomarkers at low concentrations remains a fundamental challenge. In this study, we describe an *in-silico* approach to evolve higher sensitivity peptide-based BREs for the detection of cardiac event marker protein troponin I (cTnI) from a previously identified BRE as the parental affinity peptide. The P2 affinity peptide, evolved using our *in-silico* method, was found to have ~16-fold higher affinity compared to the parent BRE and ~10 fM (0.23 pg/mL) limit of detection. The approach described here can be applied towards designing BREs for other biomarkers for human health monitoring.

KEYWORDS: troponin I, biorecognition elements, biosensor, phage displayed peptides, LSPR, computational modeling



Biomarkers are measurable indicators of a biological state and are often measured to examine biological processes. The detection of biomarkers using biosensors takes advantage of specific and high affinity biomolecular interactions, including antigen–antibody or enzyme–substrate interactions, on an active device interface to provide sensor response at low concentrations.^{1–4} The identification of biomolecular recognition elements (BREs) with high specificity and selectivity to target biomarkers remains the biggest challenge in the development of high-performance biosensors for human health monitoring and in the detection of emerging threats, such as Ebola and Zika viruses.⁵ Consequently, overcoming this challenge requires a rapid, efficient, and automated method for the design of high affinity BREs. Short peptides are appealing as BREs because of their low cost, low molecular weight, ease of synthesis, and environmental stability.^{6,7} Peptide BREs are significantly smaller than antibodies, which places them in closer proximity to the active electronic or plasmonic material surface leading to increased sensitivity in biosensors.⁸ Most peptide BREs are identified from natural sources⁹ or from combinatorial phage display libraries.¹⁰ Combinatorial ap-

proaches can be used to rapidly identify peptide binders from a large pool of sequences.^{11,12} However, phage display peptide libraries do have some limitations including library biases, parasitic sequences, and elution methods that may not necessarily result in the isolation of high-affinity peptides.¹³ The combination of phage peptide display screening along with computational modeling could be an approach to identify high affinity peptide BREs. In this study, we employ *in-silico* methods to evolve BREs from a starting parental affinity peptide identified from a phage peptide display library for cardiac troponin I (cTnI). cTnI is a biomarker of choice for assessing cardiovascular disease¹⁴ and is also of interest as an *in vivo* biomarker for stress and fatigue.¹⁵ It is widely accepted that the concentration of cTnI in blood serum is a highly sensitive and a specific biomarker for myocardial damage.^{14,16} The clinical cTnI range for at-risk patients is 0.1 to 10 ng/mL, although much lower (0.04 ng/mL) concentrations are also of interest

Received: February 20, 2018

Accepted: May 9, 2018

Published: May 9, 2018

for risk stratification.¹⁶ Enzyme-linked immunosorbent assays (ELISA) are widely used for the clinical detection of cTnI (limit of detection = 50 pg/mL).¹⁷ The time, cost, and instrumentation required for ELISA-based approaches are drawbacks for the early and rapid diagnosis of cardiac events, and several antibody-based alternatives have recently been proposed to detect cTnI in biological fluids.^{17–19} We recently demonstrated a low-cost bioplasmonic paper based device for selective and sensitive detection of cTnI⁸ using a peptide-based BRE.²⁰ The smaller sized peptide BRE provides higher sensitivity and a lower detection limit as well as excellent shelf life and improved thermal stability compared to the anti-cTnI antibody. Our current study builds upon the premise that the performance of peptide BREs can be further improved using an *in-silico* approach.

In this paper, we describe an *in-silico* method for evolving short peptide BRE sequences that bind to cTnI. Starting from a previously identified phage-display parental dodecapeptide BRE (termed P0) against cTnI,²⁰ computational search algorithms were used to scan amino acid sequences and conformational space for optimized BREs that are evaluated in atomistic molecular dynamics simulations. The *in-silico* BREs were characterized experimentally using dot-blot immunoassays, surface plasmon resonance (SPR), circular dichroism, (CD) and localized surface plasmon resonance (LSPR) (Figure 1).

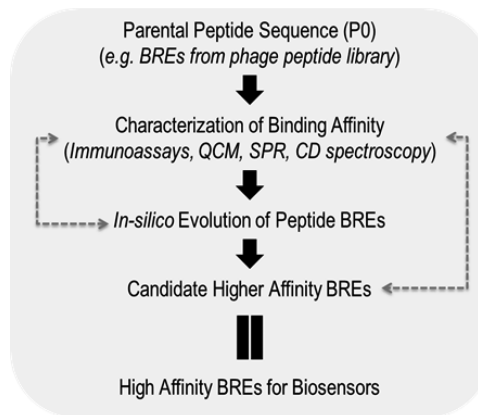


Figure 1. Schematic for evolving higher affinity peptide BREs.

We identified a peptide (termed P2) with a binding affinity for cTnI of $K_D = 0.27 \text{ nM}$, and a detection limit of 10 fM (0.2 pg/mL). The methods used in this study can be easily generalized and extended to designing high affinity BREs for other human health and performance biomarkers.

EXPERIMENTAL METHODS

Materials. All peptides were synthesized chemically by Genscript and purified to at least 95% purity. Peptides were dissolved in double deionized water to yield a stock concentration of 10 mg/mL and immediately used in order to prevent cysteine oxidation. Human cardiac troponin I full length protein (ab50803) was obtained from Abcam at a stock concentration of 1.4 mg/mL, while rabbit polyclonal Anti-cTnI antibodies (H-41) at 200 $\mu\text{g}/\text{mL}$ were purchased from Santa Cruz Biotechnology.

Computational Modeling. *In-silico* peptide evolution starts from a target complex identified from modeling by using I-TASSER²¹ to calculate the solution structure of cTnI and ZDOCK²² to identify potential peptide binding sites. Replica-exchange molecular dynamics with the AMBER force field was used to determine binding sites that are amenable to binding with peptides attached to gold surfaces.^{23,24}

The optimized peptide sequence was obtained using Monte Carlo-based software written at North Carolina State University, as previously described.^{25,26} Molecular dynamics simulations were used to evaluate the thermodynamics of the bound peptides using the AMBER force field with TIP3P water and chloride ions to neutralize the system. Additional details are provided in the Supporting Information.

Immunoblot Assay. For immunoblot, 2 μL of P0, P2, P4, and P5 peptides (10 mg/mL) and 2 μL of full length cTnI (1.4 mg/mL), as a positive control, were spotted onto a 4 in. \times 0.5 in. nitrocellulose membrane with 0.45 μm pore size (Invitrogen) about a cm apart and allowed to air-dry for 30 min. The entire membrane was then blocked by immersion in ~5 mL of Tris Buffered Saline with 0.1% Tween 20 (TBST) and 1% bovine serum albumin (BSA) in a sterile Petri dish for 2 h. During this time, the membrane was gently agitated on a rocker. After blocking, TBST with 1% BSA was removed and replaced with ~5 mL of 30 nM cTnI diluted in TBST with 1% BSA. The cTnI target (recombinant human cardiac troponin I, Life Technologies) was incubated with immobilized peptides on membrane for 4 h and agitated on a rocker. After 4 h, the cTnI in TBST with 1% BSA was removed from the membrane, and 5 mL of fresh TBST with 1% BSA was added in order to wash excess uncaptured cTnI. The membrane was washed 2 more times with fresh TBST with 1% BSA. After a total of 3 wash steps, a polyclonal human cardiac troponin I Anti-cTnI antibody (H-41, Santa Cruz Biotechnology) was added to membrane at a 1:1000 dilution in 5 mL of TBST with 1% BSA and incubated on a rocker for 12 h. After 12 h, the membrane was thoroughly washed 3 times with 5 mL of TBST with 1% BSA. Next, a goat Antirabbit secondary antibody conjugated with alkaline phosphatase was added to membrane at 1:1000 dilution in TBST with 1% BSA and incubated for 4 h. After 4 h, the membrane was washed 3 times with 5 mL of TBST and 1 time with double deionized water. Finally, these binding interactions were detected colorimetrically by exposing membrane to 3 mL of substrate (nitroblue tetrazolium/5-bromo-4-chloro-3-indolyl phosphate) for 5 min. After 5 min, the membranes were extensively washed with double deionized water and a digital color image was recorded using a point and shoot 12 MP Canon digital camera. RGB intensities were measured using ImageJ software and subtracted from background intensity for each peptide-troponin spot and averaged over an area of 514 square pixels.

Circular Dichroism Spectroscopy. Circular dichroism spectra were collected on a Jasco J-815 circular dichroism (CD) spectrometer using a 750 μL quartz cuvette from 180 to 260 nm with a data pitch of 0.1 nm, bandwidth of 1 nm, scan rate of 50 nm/min, and averaged over 3 scans. In total, we collected the CD spectra of all cTnI-binding peptides at 19 μM in water in the absence of cTnI, full length cTnI target at 19 μM in water in the absence of peptides, and the addition of peptides to cTnI to form peptide–cTnI complex (1:1) in water. The spectra of the peptide–cTnI complexes were subtracted from the reference spectra of individual cTnI-binding peptides. CDPro software was used to analyze CD spectrum according to secondary structure contribution.

Surface Plasmon Resonance. A BioNavis multiparametric surface plasmon resonance (MP-SPR) Navi 210A instrument integrated with a degasser and automated for six samples was used to measure troponin binding kinetics. Gold coated SPR sensors purchased from BioNavis were cleaned via UV-ozone treatment for 10 min, heated in a 7.5:1:1 solution of water–30% H_2O_2 – NH_4OH at 80 °C for 10 min, thoroughly rinsed with double deionized water, and dried with N_2 . The clean gold coated SPR sensors were mounted in a sensor holder and inserted into MP-SPR instrument. For immobilization of troponin-binding peptides on gold coated SPR sensors, 500 μL of peptide at a concentration of 50 $\mu\text{g}/\text{mL}$ in deionized and filtered water was injected at a flow rate of 30 $\mu\text{L}/\text{min}$ using a prewait delay time of 2 min, 10 min injection period of peptide or target, and 2–40 min postwait time to allow for peptide dissociation. During prewait and postwait periods, deionized and filtered water was flowed across peptide modified sensors at 30 $\mu\text{L}/\text{min}$ to establish stable baseline and allow dissociation. After immobilization of troponin-binding peptides on gold coated SPR sensor, 500 μL of troponin (cTnI) was injected at

multiple concentrations of 100 fM, 10 pM, 750 pM, 2 nM, 10 nM, 50 nM, and 100 nM in deionized water. For each different troponin concentration, we prepared new peptide modified sensor surfaces due to difficulty in disrupting peptide–troponin binding interaction and regenerating the surface. For calculation of K_D , we compiled the raw SPR sensograms for each troponin concentration, defined the binding association and dissociation regions, and used kinetics evaluation to fit SPR data curves using a one to one binding stoichiometry.

Electrochemical Impedance Spectroscopy. The 25 μm diameter gold electrodes were cleaned and polished using a microfiber polishing pad and 0.05 μm alumina (CH Instruments). Postpolishing, they were sonicated briefly in ethanol, followed by running 40 cyclic voltammograms in 0.1 M K_2SO_4 at pH 3 (−0.4 V to −1.8 V) followed by 40 cyclic voltammograms at pH 11 (0.4 to 1.8 V). The alkaline and acidic electrochemical cleaning steps were repeated until less than 1% change in the gold reduction peak height (~ 0.8 V vs AgCl) was observed during the acidic electrochemical cleaning step. A volume of 125 μL of 1× PBS solution containing 1 μM of 6-mercaptop-1-hexanol (Sigma-Aldrich) and 1 μM of P2 or P2 scrambled peptides were incubated with cleaned gold electrodes. The peptide coated electrodes were then rinsed and placed in a glass electrochemical cell containing 2 mL of 1× PBS containing 5 mM $\text{K}_3\text{Fe}(\text{CN})_6$ –5 mM $\text{K}_2\text{Fe}(\text{CN})_6$, a platinum coated titanium rod (EDAQ), and a Ag/AgCl reference electrode (CH Instruments). Electrochemical impedance spectroscopy (EIS) experiments were acquired using a Gamry 600 potentiostat in a CH instruments Faraday cage at a dc offset of +0.210 V vs AgCl, 10 mV ac amplitude, and a frequency range from 10 000 to 10 Hz (10 acquisition points per decade). A total of 10 spectra were acquired in order to establish a stable baseline.

Troponin was titrated in and mixed between sample additions. Pseudocircuits were fit using the Gamry Analyst software using a modified Randles cell (constant phase element instead of capacitor) with Warburg diffusion as done previously.²⁷ The values for R_2 representing the resistance to charge transfer were recorded, normalized against the blank control, and plotted against concentration. Dissociation constant was determined by fitting a Langmuir isotherm using solver from Excel to the normalized R_{CT} . The solver algorithm was setup with a constant offset value of 1 and to enable adjustment of K_a and R_{Max} in order to minimize the squared difference between the normalized R_{CT} and the calculated R_{CT} .

Localized Surface Plasmon Resonance. Gold nanorods were synthesized using a seed mediated approach.²⁸ Methods of peptide conjugation, paper substrate preparation, and extinction spectra measurements were performed as described by Tadepalli et al.⁸ AuNR–peptide conjugates were prepared by adding 8 μL of the peptide (concentration 1.31 mM in water), 2 μL at a time to a solution of 1 mL of twice centrifuged nanorods. The solution was left overnight on a shaker to homogenize the conjugation. The resulting nanorod–peptide conjugates showed a shift of ~ 1 –3 nm. A 1 cm × 1 cm filter paper (Whatman no. 1) was immersed in a solution of gold nanorods conjugates and left overnight at 4 °C. The paper strip was taken out and washed with 0.1 M Tris buffer pH 8.0 and immersed in different concentrations of troponin (Life Diagnostics) for 2 h at 4 °C. It was removed and washed thoroughly with buffer and dried under a stream of nitrogen. Scanning electron microscope images were obtained using a FEI Nova 2300 Field Emission SEM at an accelerating voltage of 10 kV. Peptides were purchased from Genscript, USA Inc. Extinction spectra from paper substrates were collected using a CRAIC microspectrophotometer (QDI 302) coupled to a Leica optical microscope (DM 4000 M) with 20× objective in the range of 450–800 nm with 10 accumulations and 100 ms exposure time in reflection mode. The spectral resolution of the microspectrophotometer is 0.2 nm. Multiple UV–visible spectra (~ 10) were collected from different locations of the paper strip before and after exposure to each troponin concentration. The gold paper was incubated in 250 μL of troponin at each concentration for 2 h and air-dried before measurements were taken. A Shimadzu UV-1800 spectrophotometer was employed to collect UV–vis extinction spectra from solution.

RESULTS AND DISCUSSION

Modeling the cTnI–Peptide Interactions. The cTnI starting structure was reconstructed (Figure S1) from the partial crystal structure of troponin I in the troponin C/troponin T/troponin I complex (PDB 1J1E)²⁹ using I-TASSER homology modeling.²¹ The initial structure for *in-silico* evolution was generated by docking the parental troponin-binding peptide (P0, FYSHSFHENWPS; $K_D = 17$ nM)²⁰ onto the model cTnI structure using the ZDOCK package.²² Two potential binding sites within cTnI, amino acid residues 69–111 and 114–144, were identified in the docking studies for peptide P0. We chose to focus on the cTnI (114–144) binding site (Figure 2A) since the binding conformation at this site was

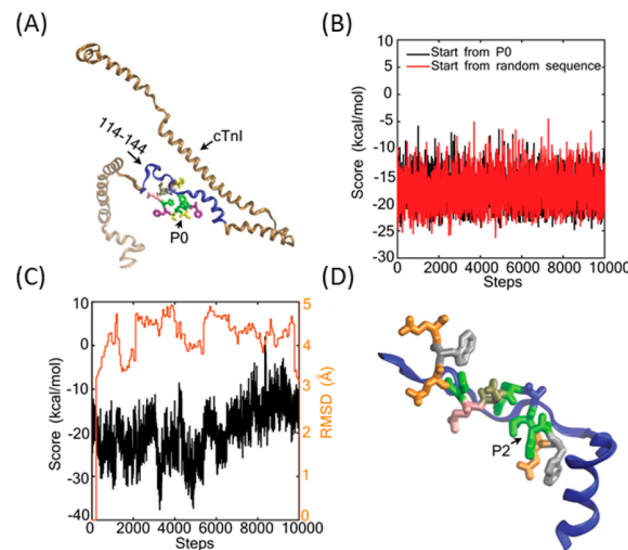


Figure 2. Computational modeling of cTnI–peptide complex. (A) Structure of P0 peptide bound to cTnI (the binding region shown in blue), (B) plots of score vs steps with sequence evolution only starting from the known P0 and random sequences, respectively, resulting in evolved peptides, (C) score (black trace) and RMSD (red trace) vs steps during sequence evolution with conformational change starting from random sequence. (D) Structure of *in-silico* evolved P2 peptide bound to the amino acid region 114–144 of the cTnI (shown in blue).

previously determined.⁸ The binding site was also further validated by comparing the binding affinities of peptide P0 to the full cTnI protein and to the cTnI (114–144) fragment ($K_D = 4.30 \pm 0.13 \times 10^{-2}$ nM for the full cTnI; $K_D = 2.76 \pm 0.11 \times 10^{-2}$ nM for the fragment; see Table 2). Consequently, we chose the fragment cTnI (114–144) as the binding target to search for the optimized recognition peptides. This model was validated in studies comparing the binding of optimized peptides to cTnI and cTnI (114–144) (*vide infra*).

Computational Peptide Design. The sequence and conformation of the optimized cTnI binding peptides were determined using the computational peptide design algorithm (Figure S2). The affinity of each peptide binder to cTnI is evaluated using a score function,³⁰ which takes into account both the binding energy of the peptide-cTnI (114–144) complex and the energy of the peptide when stabilized in the bound conformation, using a fixed conformation for cTnI (114–144). Sequence evolution is conducted with and without conformation change in evolving the peptides. When no conformation change is involved, the search process starts from either the original parental peptide P0 or a random sequence

Table 1. Thermodynamic Parameters Extracted from a 40 ns Explicit-Solvent Molecular Dynamics Simulation and Scores Obtained from the Peptide Design Algorithm

peptide	sequences	Γ_{score}	$\Delta G^{\text{avg}}_{\text{binding}}$ (kcal/mol)	$\Delta H^{\text{avg}}_{\text{binding}}$ (kcal/mol)	$T\Delta S^{\text{avg}}_{\text{binding}}$ (kcal/mol)
P0	FYSHSFHENWPS	-14.57	-7.57 ± 0.18	-32.44 ± 0.13	-24.87 ± 0.12
P1	LQQWATNEHQWY	-26.12	-7.58 ± 0.18	-35.40 ± 0.12	-27.82 ± 0.14
P2	HWQIAYNEHQWQ	-26.56	-15.00 ± 0.19	-46.47 ± 0.15	-31.47 ± 0.13
P3	NQWWFQNEHWPN	-42.55	0.02 ± 0.16	-23.83 ± 0.15	-23.85 ± 0.06
P4	QIAQHVQEHHMIQ	-37.75	-14.21 ± 0.18	-40.70 ± 0.17	-26.49 ± 0.11
P5	WWTFMANEHQQH	-39.45	-12.98 ± 0.18	-38.30 ± 0.17	-25.33 ± 0.11
P6	HWQNAYNDHMIQ	-38.46	-6.93 ± 0.18	-33.99 ± 0.14	-27.06 ± 0.12
PC	HWNMAANEHMQW	-25.58	-0.58 ± 0.18	-23.67 ± 0.16	-23.09 ± 0.10

peptide with the same mix of hydrophobic and hydrophilic residues. When conformation change is involved, the search process always starts from a random peptide sequence. Two parameters, δ_{\max} and $kT_{\text{conformation}}$, are used to control the magnitude of the conformation change moves. The parameter δ_{\max} is the allowable maximum root-mean-square deviation (RMSD) of the new peptide backbone conformation relative to the initial peptide backbone conformation, and the $kT_{\text{conformation}}$ controls the likelihood that a new peptide conformation will be accepted, with higher values making acceptance easier. A constraint placed on the *in-silico* evolution process is that the number of positively charged, negatively charged, hydrophobic, polar, and other amino acid types in all evolved peptides remain the same as in the starting parental sequence P0. The algorithm was developed initially using the Amber force field 99SB but is also compatible with recent updated versions, such as Amber ff12 and Amber ff14. The peptide design results from the algorithm using the three Amber force fields were found to be identical. The algorithm could, in principle, be used to generate novel peptide binders of any length, provided that the binding site of the target of interest is known or predetermined. Of course, evolving a long peptide takes more computing time. A typical evolution profile for the peptide search in the absence of conformational change is shown in Figure 2B, while the evolution profile for the peptide search in the presence of conformational change at ($\delta_{\max}, kT_{\text{conformation}}$) = (5.0, 3.0) is shown in Figure 2C. The large fluctuations in the RMSD plot show that this method samples a sufficiently broad region of conformational space to identify new peptide sequences. To avoid local searches, we performed a series of sequence evolutions at different sets of values of parameters ($\delta_{\max}, kT_{\text{conformation}}$), including (4.0, 3.0), (5.0, 3.0), (4.0, 4.0), and (5.0, 4.0). The top sequences were further evaluated using molecular dynamics simulations (40 ns) in explicit solvent, and Table 1 lists the calculated scores and binding free energies for the phage-display peptide (P0), the six peptides identified by *in-silico* evolution (P1–P6) and a negative control sequence (PC).

The simulated structure of the top evolved peptide (P2) bound to cTnI (114–144) is shown in Figure 2D. The calculated binding free energy (ΔG) of the parental peptide P0 is 7.57 ± 0.18 kcal/mol, while the *in-silico* evolved peptide P2 has the lowest binding free energy (15.00 ± 0.19 kcal/mol). The comparison of evolved sequences to the parental peptide P0 sequence using the ClustalW2 sequence alignment tool is shown in Figure 3. The ClustalW2 tool is commonly used to highlight regions of similarity that are more highly conserved than other regions within a set of proteins or peptides.³¹ The amino acids in position 7–9 in all the dodecapeptides are mostly conserved, with the charged and polar residues maintained in all of the evolved sequences. Divergence in the

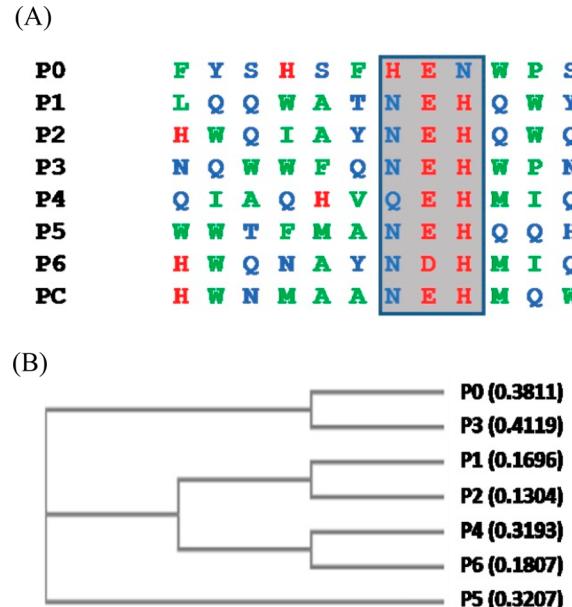


Figure 3. *In-silico* evolved sequence analysis. (A) ClustalW sequence alignment of the peptide sequences (<http://www.ebi.ac.uk/Tools/msa/clustalw2/>). Shaded box shows the highly conserved amino acids. Color classification of amino acids- polar (blue), hydrophobic (green) and charged (red). (B) Cladogram showing the relationships and distances based on amino acid sequences was obtained using Kalign sequence alignment tool (<http://www.ebi.ac.uk/Tools/msa/kalign/>).

position of hydrophobic, charged, and polar amino acid residues can be seen in the flanking regions (positions 1–6 and 10–12) (Figure 3A). For example, the parental P0 peptide has a polar N-termini and a hydrophobic C-termini, while P2 peptide has a hydrophobic N-termini and a polar C-termini. We also classified the evolved peptide sequences using a cladogram that shows the “evolutionary” relationships between the sequences using Kalign sequence alignment tool to derive the relationships between the *in-silico* evolved sequences using a phylogenetic analysis (www.expasy.ch). Kalign employs an approximate string-matching algorithm to calculate sequence distances by incorporating local sequence matches into the alignment.³² Pairwise distances are first calculated by alignment of the most similar sequences, and then the tree is constructed by the order of pairwise alignments of the sequences. As shown in Figure 3B, the parental peptide sequence P0 is aligned more closely with peptide P3 while P1, P2, P4, and P6 more closely associated with each other (Figure 3B). This classification also aids in selecting evolved peptide sequences from separate clusters for further analysis. We selected evolved affinity peptides P2, P4, and P5 for further analysis and compared it

to the phage peptide library identified parental affinity peptide P0.

Validation of Evolved Peptide BREs. The recognition and affinities of evolved peptides for cTnI were evaluated using dot-blot immunoassays, SPR, CD, and LSPR spectroscopy. We first confirmed the recognition of cTnI by the *in-silico* evolved peptides using a dot-blot immunoassay as a rapid screening tool (Figure S3). In Figure 4A, we plot the intensity of the dot-blot

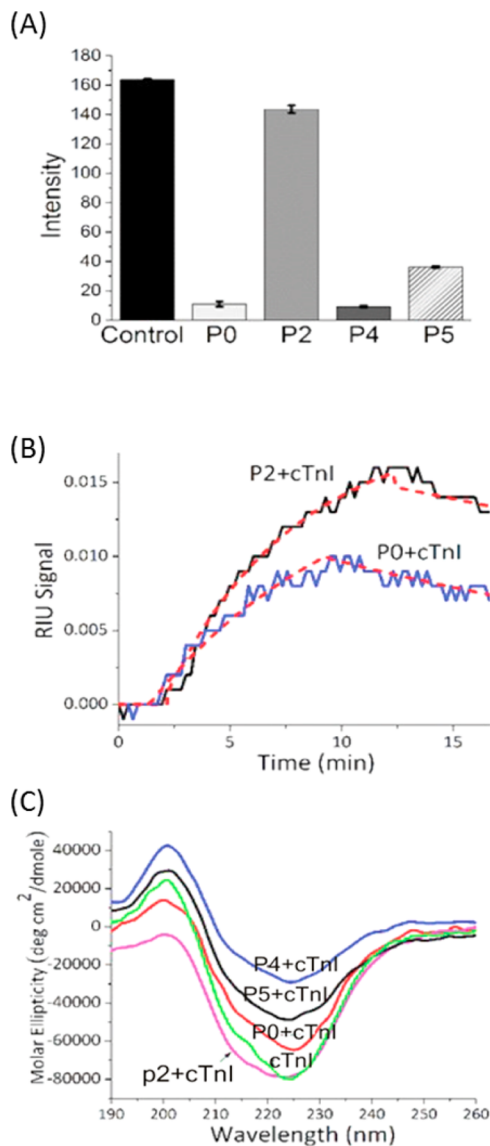


Figure 4. Characterization of evolved peptide BREs. (A) Signal intensity of dot-blot immunoassay for cTnI binding, control shown is for anti-cTnI antibody. (B) Representative SPR spectra for P0 and P2 peptide binding to 2 nM cTnI. RIU = refractive index unit and (C) CD spectra showing the effect of peptide binding on the secondary structure of cTnI.

immunoassay signal for the parental, evolved peptide, and anti-cTnI antibody. The results demonstrate that the evolved peptides recognize and bind to cTnI. Qualitatively, the binding strengths of troponin-binding peptides can be ranked as to $P_2 \gg P_5 > P_0 \geq P_4$ based on the signal intensities. The anti-cTnI antibody was used as a positive “gold standard” control which had the highest signal intensity as expected. Although the immunoblot assays allows for confirming the recognition and

binding of the evolved peptides, multiparametric SPR (MP-SPR) was used to quantitatively measure the binding affinities of the *in-silico* cTnI-binding peptides. The binding affinities of the evolved peptides, parental peptide P0, a negative peptide control (PC), and the anti-cTnI antibody were measured. The peptides of interest (P0, P2, P4, and P5, and PC) were modified with a C-terminal cysteine for immobilization on the gold surface of the SPR sensor chip and a three-residue glycine spacer to extend the peptides from the SPR sensor chip surface (Figure S4). Immobilization of troponin-binding peptides on a gold surface (0.16 cm^2) resulted in peptide densities of 190 ng/cm^2 to 260 ng/cm^2 for the set of peptides, thicknesses of $\sim 1.8 \text{ nm}$, and $>85\%$ surface coverage of peptides on gold (Figure S5). This high surface coverage of peptides reduces the likelihood of nonspecific adsorption of cTnI to the gold surface. After immobilization, the peptide-modified sensors were then exposed to varying concentrations of cTnI and the SPR response was recorded under ligand depletion conditions (i.e., high effective probe concentration on surface, low sample volumes).³³ Under these conditions, peptide-troponin binding favors low target concentrations, high peptide-troponin affinities, and low receptor occupancies. For the latter, maximum occupancy of peptides is $\sim 1\%$ at full saturation of troponin on the sensor surface. In this case, low receptor occupancy is dictated by the high molecular weight and large molecular footprint of cTnI compared to the small peptide size (Figure S5). SPR spectra are shown in Figure 4B for the P2 and P0 peptides. The representative binding affinities for cTnI and cTnI (114–144) are shown in Table 2. The cTnI binding

Table 2. Binding Constants of Peptides to Full Length cTnI and Fragment 114–141 of cTnI As Measured by MP-SPR

peptide	K_D cTnI nM	K_D cTnI 114–141 nM
P0	4.30 ± 0.0010	2.76 ± 0.001
P2	0.27 ± 0.0001	0.44 ± 0.001
P4	1.03 ± 0.0010	3.03 ± 0.003
P5	3.39 ± 0.0500	4.12 ± 0.001
anti-cTnI	0.12 ± 0.0001	10.70 ± 0.007

affinity of the parental P0 peptide was determined to be 4.3 nM by SPR. This is 4-fold higher than the previously reported value of 17 nM measured by quartz-crystal microbalance.²⁰ The increase in binding affinity is most likely due to the more sensitive SPR-based detection technique as compared to the QCM used in the previous study.²⁰ Using the SPR binding affinity value of P0 peptide as the baseline, we observed that the P2 peptide shows the highest affinity for cTnI (0.27 nM) with a ~ 16 -fold higher affinity for cTnI compared to P0. The peptides P4 and P5 have lower affinities (1.0 and 3.4 nM) than P2 but are still strong binders as compared to peptide P0. The control peptide PC showed no significant response in the SPR binding assay and the binding affinity could not be measured (Figure S6). Similarly, we observed a 100-fold decrease in binding affinity ($K_D = 21.2 \text{ nM}$) when P2 was randomly scrambled (YQEWIQHNWAQH).

We also used electrochemical impedance spectroscopy (EIS) to confirm the binding affinity of P2 peptide to cTnI. Due to the portability of EIS circuitry and the promise of near real-time detection, it has been proposed for use in wearable sensors. EIS and its similar impedance-based methodologies have been used in many cases to both demonstrate binding to an affinity ligand^{34,35} and to fabricate electrochemical sensors by inter-

rogating the impedance of the redox couple to the probe surface containing the active sensing element.³⁶ Similarly, as cTnI bound to P2 peptide, the fluidic resistance (18.2 M Ω for water or 13.2 k Ω for 1× PBS) to redox couple diffusion increased, resulting in an increase in resistance to charge transfer (R_{CT}). Since multiple factors impact impedance, including surface roughness, distance from the electrodes, etc., the ratio between the blank (R_{CT^0}) and the sample R_{CT^*} was plotted. The experimental data showed a large increase in the ratio of R_{CT^*}/R_{CT^0} for P2 coated electrodes compared to the control with cTnI (Figure S7). Fitting of the EIS binding curve to a Langmuir isotherm yielded a K_D of 0.34 nM which is in close agreement with the SPR measurement. By comparison, we observed a negligible signal change for the scrambled P2 control peptide (Figure S7). The fact that the P2 peptide shows similar affinity (0.44 nM) toward the cTnI fragment validates our modeling assumptions that the peptide binding site lies within the cTnI (114–144) fragment. It is of interest to note that the cTnI antibody has a much lower affinity for the cTnI (114–144) fragment compared to the full protein (10.7 vs 0.12 nM) as shown in Table 2. This indicates that the *in-silico* evolved peptides bind to a site on cTnI that differs from that of the cTnI antibody. This finding has important implications for using the *in-silico* evolved peptides in combination with antibodies for biosensor design.

Circular dichroism (CD) spectroscopy is widely used to explore the secondary structure of proteins.³⁷ We explore whether the binding of the affinity peptides has an effect on the secondary structure of cTnI. The CD spectra for cTnI is dominated by negative peaks at 222 and 208 nm. This represents the classical CD signature for the α -helix in proteins³⁷ and is consistent with the high α -helical fraction found in the crystal structure of cTnI.²⁹ CD measurements on the short peptides (P0, P2, P4, and P5) are expected to be unstructured in solution with a broad negative feature centered at ~195 nm, characteristic of random coil conformations. The addition of P0 to cTnI resulted in ~10% loss of helicity and an 18% increase in unordered structure of cTnI, based on deconvolution of CD spectrum (Figure 4C). The addition of peptide P2 resulted in a 5% loss in helicity, a 22% increase in unordered structure, and a loss of β -turns of cTnI, while the P4 peptide produced a 27% loss in helicity upon binding to cTnI (Figure S9). Together, the CD studies suggest that peptide binding leads to disruption in secondary structure of cTnI and further demonstrates binding of the evolved peptides to cTnI.

Biosensors based on changes in the plasmonic absorbance for metal nanostructures are increasingly attractive as low cost, field-deployable, and flexible biodiagnostic devices.³⁸ We recently demonstrated a low-cost paper-based LSPR device for the detection of cTnI using P0 as the affinity BRE to selectively detect cTnI in biological fluids.⁸ These earlier studies showed the enhanced environmental stability of paper-based devices and a lower limit of detection (LOD) using peptide BREs as compared to the anti-cTnI antibody. Using a paper-based bioplasmonic device, we compare the binding affinity and LOD of the parental P0 peptide to the *in-silico* evolved peptides. The paper-based devices were prepared using a previously established method.⁸ As in the SPR experiments, the dodecamer peptides were extended with three glycines and a C-terminal cysteine to facilitate coupling to the gold nanorod (AuNR) surface. The conjugation of the peptide to the gold nanorod was confirmed by a small (~1–3 nm) red shift in the LSPR spectrum. The SEM image of the paper revealed a

uniform distribution of the bioconjugated AuNRs with no signs of aggregation or patchiness (Figure 5A), and the areal density

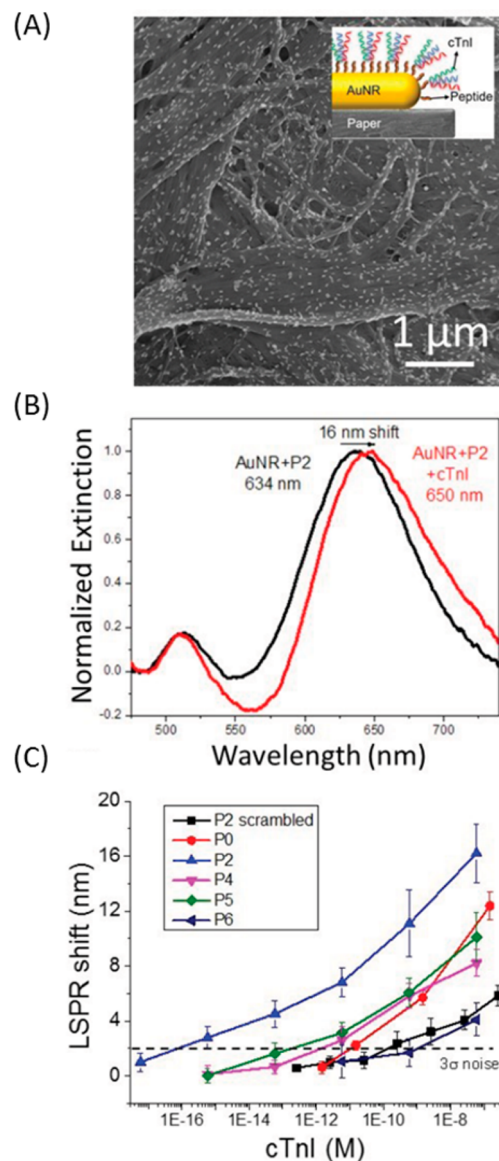


Figure 5. Peptide-functionalized bioplasmonic paper device for sensing cTnI. (A) SEM image depicting the uniform adsorption of peptide BRE-conjugated gold nanorods on paper substrate. Schematic showing the process for cTnI-peptide on gold nanorod immobilized on paper (inset). (B) Extinction spectra showing the LSPR shift after addition of cTnI to 0.1 M TBS (pH 8) using P2 peptide as the BRE. (C) Sensing calibration curves of cTnI spiked in buffer using the *in-silico* evolved peptides. The 3σ noise level is shown (dashed line).

of the BRE-conjugated AuNRs was similar in all samples. The longitudinal LSPR band (~630 nm) is used for detecting and monitoring the target binding events because of its higher refractive index sensitivity compared to the transverse LSPR band.³⁹ At high cTnI concentrations (58 nM) LSPR red shift as large as 16 nm could be observed for the plasmonic paper modified with the P2-conjugated AuNRs (Figure 5B). The limit of detection (LOD) in plasmonic paper sensor is determined by the minimum shift that can be reliably measured upon target binding and is 3σ over the background signal. The effect of cTnI concentration on the LSPR shift for the peptide-modified

plasmonic paper is shown in Figure 5C. In total, these data show that the LODs for P0, P4, P5, and P6 are \sim 20 pM. In contrast, the LSPR device using P2 peptide as the BRE showed a limit of detection of \sim 10 fM (0.23 pg/mL), which is nearly 3 orders of magnitude lower than for P0 peptide. Moreover, we were able detect a red shift of $>$ 2 nm with even lower concentrations of cTnI (\sim 1 fM or 0.02 pg/mL). The large molecular size footprint of full length troponin in combination with high affinity peptides enables femtomolar detection limits at low occupancy of peptides. By comparison, we determined an LOD for the cTnI antibody, using the LSPR device, of 353 pM (8 ng/mL).⁸ This value is consistent with the previously reported LOD of 10 ng/mL using a similar nanorod based LSPR measurement.⁴⁰

CONCLUSIONS

In this study we demonstrate the use of *in-silico* methods to evolve peptides as BREs for biosensing applications. Starting with a parental peptide (P0) shown to specifically bind the target (cTnI) identified from a phage peptide display library, we applied an *in-silico* peptide evolution method to aid in the identification of higher affinity peptide BREs. cTnI, important marker for cardiac disease, was used as our model biomarker and *in-silico* evolved P2 peptide incorporated into a bioplasmonic sensing device demonstrated an extremely low LOD compared to the parental P0 peptide.

The increased sensitivity of peptides BREs can be attributed to its smaller size which puts it in close proximity to the plasmonic nanorod surface maximizing sensitivity to the electromagnetic field, enabling larger changes to the LSPR peak. The 12-mer peptides identified here are much smaller than typical antibodies and locate the BRE-target interactions to be close in proximity to the active sensing surface, leading to a higher sensitivity and lower LOD. Although the current experiments focused on cTnI, the methods are generalizable and could be extended to a wide variety of protein, peptide, and small molecule targets provided that there are starting sequences.

Future efforts will be directed toward automation to enable rapid BRE discovery for a wide variety of diseases, performance markers, and chemical threats. The success of our algorithm to design higher affinity peptide BREs for cTnI depends in part on the ability to locate a promising binding site on the target protein. The location of a likely binding site on cTnI was obtained using molecular modeling, docking, and simulation based on the parental phage-display discovered peptide. Knowledge of the location of the binding site allows us to search for potential peptide binders for cTnI in a rapid and effective manner. All the experimentally proven high-affinity peptides P2, P4, and P5 were obtained via the algorithm based on the amino acid composition of the parental P0 peptide sequence. The application of our algorithm is limited to systems wherein the location of a peptide binding site on the target molecule is either available or can be predicted. Peptide BREs have significant advantages over antibodies in terms of cost, environmental stability, and shelf life. Peptide BREs identified from combinatorial libraries against a biomarker of interest can be further improved on using a computationally based evolution method as described here. This would lead to the rapid development of high affinity BREs for fabricating sensitive and selective biosensors.

ASSOCIATED CONTENT

S Supporting Information

The Supporting Information is available free of charge on the ACS Publications website at DOI: [10.1021/acssensors.8b00159](https://doi.org/10.1021/acssensors.8b00159).

Computational and experimental methods, MP-SPR sensograms, and EIS and CD data ([PDF](#))

AUTHOR INFORMATION

Corresponding Authors

*E-mail: rajesh.naik@us.af.mil.

*E-mail: hall@ncsu.edu.

ORCID

Steve Kim: [0000-0002-9519-077X](https://orcid.org/0000-0002-9519-077X)

Peter A. Mirau: [0000-0002-5210-4990](https://orcid.org/0000-0002-5210-4990)

Carol K. Hall: [0000-0002-7425-587X](https://orcid.org/0000-0002-7425-587X)

Rajesh R. Naik: [0000-0002-7677-928X](https://orcid.org/0000-0002-7677-928X)

Notes

The authors declare no competing financial interest.

ACKNOWLEDGMENTS

We acknowledge support from Air Force Office of Scientific Research (S.S. Award No. FA9550-15-1-0228, C.K.H. Award No. FA9550-16-10078, R.R.N Award No. 12RX11COR) and AFRL/RX, and AFRL/711 HPW. This work used the Extreme Science and Engineering Discovery Environment (XSEDE), which is supported by National Science Foundation Grant Number ACI-1053573. X.X. and C.H.K. thank Texas Advanced Computing Center (TACC) and San Diego Supercomputer Center (SDSC) for providing us computing time.

REFERENCES

- (1) Huang, W. G.; Diallo, A. K.; Dailey, J. L.; Besar, K.; Katz, H. E. Electrochemical processes and mechanistic aspects of field-effect sensors for biomolecules. *J. Mater. Chem. C* **2015**, *3*, 6445–6470.
- (2) Tiwari, J. N.; Vij, V.; Kemp, K. C.; Kim, K. S. Engineered Carbon-Nanomaterial-Based Electrochemical Sensors for Biomolecules. *ACS Nano* **2016**, *10*, 46–80.
- (3) Zhang, A.; Lieber, C. M. Nano-Bioelectronics. *Chem. Rev.* **2016**, *116*, 215–257.
- (4) Zhang, S.; Geryak, R.; Geldmeier, J.; Kim, S.; Tsukruk, V. V. Synthesis, Assembly, and Applications of Hybrid Nanostructures for Biosensing. *Chem. Rev.* **2017**, *117*, 12942–13038.
- (5) Sanchez-Purra, M.; Carre-Camps, M.; de Puig, H.; Bosch, I.; Gehrke, L.; Hamad-Schifferli, K. Surface-Enhanced Raman Spectroscopy-Based Sandwich Immunoassays for Multiplexed Detection of Zika and Dengue Viral Biomarkers. *ACS Infect. Dis.* **2017**, *3*, 767–776.
- (6) Kim, S. S.; Kuang, Z. F.; Ngo, Y. H.; Farmer, B. L.; Naik, R. R. Biotic-Abiotic Interactions: Factors that Influence Peptide-Graphene Interactions. *ACS Appl. Mater. Interfaces* **2015**, *7*, 20447–20453.
- (7) Kuang, Z. F.; Kim, S. N.; Crookes-Goodson, W. J.; Farmer, B. L.; Naik, R. R. Biomimetic Chemosensor: Designing Peptide Recognition Elements for Surface Functionalization of Carbon Nanotube Field Effect Transistors. *ACS Nano* **2010**, *4*, 452–458.
- (8) Tadepalli, S.; Kuang, Z. F.; Jiang, Q. S.; Liu, K. K.; Fisher, M. A.; Morrissey, J. J.; Kharasch, E. D.; Slocik, J. M.; Naik, R. R.; Singamaneni, S. Peptide Functionalized Gold Nanorods for the Sensitive Detection of a Cardiac Biomarker Using Plasmonic Paper Devices. *Sci. Rep.* **2015**, *5*, 16206.
- (9) Slocik, J. M.; Moore, J. T.; Wright, D. W. Monoclonal Antibody Recognition of Histidine-Rich Peptide Encapsulated Nanoclusters. *Nano Lett.* **2002**, *2*, 169–173.

- (10) Molek, P.; Strukelj, B.; Bratkovic, T. Peptide Phage Display as a Tool for Drug Discovery: Targeting Membrane Receptors. *Molecules* **2011**, *16*, 857–887.
- (11) Petrenko, V. A. Evolution of phage display: from bioactive peptides to bioselective nanomaterials. *Expert Opin. Drug Delivery* **2008**, *5*, 825–836.
- (12) Wu, C. H.; Liu, I. J.; Lu, R. M.; Wu, H. C. Advancement and applications of peptide phage display technology in biomedical science. *J. Biomed. Sci.* **2016**, *23*, 8.
- (13) Derda, R.; Tang, S. K. Y.; Li, S. C.; Ng, S.; Mattock, W.; Jafari, M. Diversity of Phage-displayed libraries of peptides During Panning and Amplification. *Molecules* **2011**, *16*, 1776–1803.
- (14) White, H. D.; Thygesen, K.; Alpert, J. S.; Jaffe, A. S. Clinical implications of the Third Universal Definition of Myocardial Infarction. *Postgrad. Med. J.* **2014**, *90*, 502–510.
- (15) Debold, E. P. Recent Insights into the Molecular Basis of Muscular Fatigue. *Med. Sci. Sports Exercise* **2012**, *44*, 1440–1452.
- (16) Mahajan, V. S.; Jarolim, P. How to Interpret Elevated Cardiac Troponin Levels. *Circulation* **2011**, *124*, 2350–2354.
- (17) Han, X.; Li, S.; Peng, Z.; Othman, A. M.; Leblanc, R. Recent Development of Cardiac Troponin I Detection. *ACS Sensors* **2016**, *1*, 106–114.
- (18) Kim, K.; Park, C.; Kwon, D.; Kim, D.; Meyyappan, M.; Jeon, S.; Lee, J.-S. Silicon nanowire biosensors for detection of cardiac troponin I (cTnI) with high sensitivity. *Biosens. Bioelectron.* **2016**, *77*, 695–701.
- (19) Sun, T.; Kan, S.; Marriott, G.; Chang-Hasnain, C. High-contrast grating resonators for label-free detection of disease biomarkers. *Sci. Rep.* **2016**, *6*, 27482.
- (20) Park, J. P.; Cropek, D. M.; Banta, S. High Affinity Peptides for the Recognition of the Heart Disease Biomarker Troponin I Identified Using Phage Display. *Biotechnol. Bioeng.* **2010**, *105*, 678–686.
- (21) Roy, A.; Kucukural, A.; Zhang, Y. I-TASSER: a unified platform for automated protein structure and function prediction. *Nat. Protoc.* **2010**, *5*, 725–738.
- (22) Pierce, B. G.; Wiehe, K.; Hwang, H.; Kim, B. H.; Vreven, T.; Weng, Z. ZDOCK server: interactive docking prediction of protein-protein complexes and symmetric multimers. *Bioinformatics* **2014**, *30*, 1771–1773.
- (23) Hornak, V.; Abel, R.; Okur, A.; Strockbine, B.; Roitberg, A.; Simmerling, C. Comparison of multiple amber force fields and development of improved protein backbone parameters. *Proteins: Struct., Funct., Genet.* **2006**, *65*, 712–725.
- (24) Nelson, M. T.; Humphrey, W.; Gursoy, A.; Dalke, A.; Kale, L. V.; Skeel, R. D.; Schulten, K. NAMD: A parallel, object oriented molecular dynamics program. *International Journal of Supercomputer Applications and High Performance Computing* **1996**, *10*, 251–268.
- (25) Xiao, X. Q.; Agris, P. F.; Hall, C. K. Designing Peptide Sequences in Flexible Chain Conformations to Bind RNA: A Search Algorithm Combining Monte Carlo, Self-Consistent Mean Field and Concerted Rotation Techniques. *J. Chem. Theory Comput.* **2015**, *11*, 740–752.
- (26) Xiao, X. Q.; Wang, Y.; Leonard, J.; Hall, C. K. Extended Concerted Rotation Technique Enhances the Sampling Efficiency of the Computational Design Algorithm. *J. Chem. Theory Comput.* **2017**, *13*, 5709–5720.
- (27) Vogt, S.; Su, Q.; Gutiérrez-Sánchez, C.; Noll, G. Critical View on Electrochemical Impedance Spectroscopy Using Ferri/Ferrocyanide Redox Couple at Gold Electrodes. *Anal. Chem.* **2016**, *88*, 4383–4390.
- (28) Orendorff, C. J.; Gearheart, L.; Jana, N. R.; Murphy, C. J. Aspect ratio dependence on surface enhanced Raman scattering using silver and gold nanorod substrates. *Phys. Chem. Chem. Phys.* **2006**, *8*, 165–170.
- (29) Takeda, S.; Yamashita, A.; Maeda, K.; Maeda, Y. Structure of the core domain of human cardiac troponin in the Ca²⁺-saturated form. *Nature* **2003**, *424*, 35–41.
- (30) Xiao, X. Q.; Agris, P. F.; Hall, C. K. Introducing folding stability into the score function for computational design of RNA-binding peptides boosts the probability of success. *Proteins: Struct., Funct., Genet.* **2016**, *84*, 700–711.
- (31) Larkin, M. A.; Blackshields, G.; Brown, N. P.; Chenna, R.; McGettigan, P. A.; McWilliam, H.; Valentin, F.; Wallace, I. M.; Wilm, A.; Lopez, R.; Thompson, J. D.; Gibson, T. J.; Higgins, D. G. Clustal W and clustal X version 2.0. *Bioinformatics* **2007**, *23*, 2947–2948.
- (32) Lassmann, T.; Sonnhammer, E. L. L. Kalign - an accurate and fast multiple sequence alignment algorithm. *BMC Bioinf.* **2005**, *6*, 298.
- (33) Fernandez de Avila, B.; Watkins, H.; Pingarron, J.; Plaxco, K.; Palleschi, G.; Ricci, F. Determination of the Detection Limit and Specificity of Surface-Based Biosensors. *Anal. Chem.* **2013**, *85*, 6593–6597.
- (34) Aliakbarinodehi, N.; Jolly, P.; Bhalla, N.; Miodek, A.; De Michelis, G.; Estrela, P.; Carrara, S. Aptamer-Based Field-Effect Biosensor for Tenofovir Detection. *Sci. Rep.* **2017**, *7*, 44409.
- (35) Kumar, L.; Wang, X.; Hagen, J. A.; Naik, R.; Papautsky, I.; Heikenfeld, J. Label Free Nano-Aptamer for Interleukin 6 in Protein-Diluted Bio Fluids such as Sweat. *Anal. Methods* **2016**, *8*, 3440–3444.
- (36) Arroyo-Curas, N.; Somerson, J.; Vieira, P.; Ploense, K.; Kippin, T.; Plaxco, K. W. Real-Time Measurement of Small Molecules Directly in Awake Ambulatory Animals. *Proc. Natl. Acad. Sci. U. S. A.* **2017**, *114*, 645–650.
- (37) Greenfield, N.; Fasman, G. D. Computed Circular Dichroism Spectra for the Evaluation of Protein Conformation. *Biochemistry* **1969**, *8*, 4108–4116.
- (38) Schmucker, A. L.; Tadepalli, S.; Liu, K.-K.; Sullivan, C. J.; Singamaneni, S.; Naik, R. R. Plasmonic paper: a porous and flexible substrate enabling nanoparticle-based combinatorial chemistry. *RSC Adv.* **2016**, *6*, 4136–4144.
- (39) Chen, H.; Kou, X.; Yang, Z.; Ni, W.; Wang, J. Shape- and Size-Dependent Refractive Index Sensitivity of Gold Nanoparticles. *Langmuir* **2008**, *24*, 5233–5237.
- (40) Guo, Z. R.; Gu, C. R.; Fan, X.; Bian, Z. P.; Wu, H. F.; Yang, D.; Gu, N.; Zhang, J. N. Fabrication of Anti-human Cardiac troponin I immunogold Nanorods for Sensing Accute Myocardial Damage. *Nanoscale Res. Lett.* **2009**, *4*, 1428–1433.